Average echoes from randomly oriented random-length finite cylinders: Zooplankton models

Timothy K. Stanton and Dezhang Chu
Department of Applied Ocean Physics and Engineering, Woods Hole Oceanographic Institution, Woods Hole, Massachusetts 02543

Peter H. Wiebe
Department of Biology, Woods Hole Oceanographic Institution, Woods Hole, Massachusetts 02543

Clarence S. Clay
Department of Geology and Geophysics, University of Wisconsin, Madison, Wisconsin 53706

(Received 30 October 1992; accepted for publication 2 July 1993)

By heuristically extending the previously developed ray solution [Stanton *et al.* J. Acoust. Soc. Am. **94**, 3454–3462 (1993)] to predict the scattering by cylinders over *all* angles of incidence, approximate expressions are derived which describe the echo energy due to sound scattered by finite cylinders averaged over orientation and length. Both straight and bent finite length cylinders of high aspect ratio are considered over the full range of frequencies (Rayleigh through geometric scattering). The results show that for a sufficiently broad range of orientation, the average echo is largely independent of the degree of bend—that is, the results are essentially the same for both the straight and bent cylinders of various radii of curvature (provided the bend is not too great). Also, in the limit of high frequency (i.e., the acoustic wavelength is much smaller than the cross-sectional radius of the object), the averages are independent of frequency. The resultant formulas derived herein are useful in describing the scattering by elongated zooplankton whose shape may not necessarily be known in the natural ocean environment. The average echo is shown to depend directly upon standard deviation (s.d.) of the angle of orientation as well as size. If independent measurements of size are made (such as from trawling samples), then the properties of the angle distribution and hence behavior may be inferred from the data. Averages over both angle and a narrow distribution of size are shown to only partially smooth out deep nulls in the scatter versus frequency curves. The formulas compare favorably with laboratory data involving aggregations of animals and a broad range of frequencies (38 kHz to 1.2 MHz).

PACS numbers: 43.20.Fn, 43.30.Gv, 43.30.Xm

LIST OF SYMBOLS

p_{scat}	scattered pressure
$\mathscr{R}_{12}$	plane-wave/plane interface reflection coefficient
1,2	subscripts to k, $\mathscr{R}$, ρ, and T indicating medium "1" (surrounding fluid) and medium "2" (body medium)
T_{12}, T_{21}	transmission coefficients for planar interface due to incident plane wave
I	term describing interference between echoes from front and back interfaces of cylinder
k	acoustic wavenumber ($=2\pi/\lambda$)
λ	acoustic wavelength
a	radius of cylinder cross section
$\bar{a}$	average radius of cylinder cross section
$\bar{a}_t$	average radius of animal thorax cross section
L	length of straight finite object, arc length of uniformly bent cylinder
$\bar{L}$	average length
P_0	amplitude of incident plane wave
r	distance from cylinder to the field (measurement) point (i.e., range)
i	$\sqrt{-1}$
f	scattering amplitude for finite-sized objects
σ_{bs}	backscattering (differential) cross section
f_0, $(\sigma_{bs})_0$	scattering amplitude and backscattering (differential) cross section for normal or broadside incidence
Δ	$k_1 L \sin\theta$
$\mathscr{S}_\theta$	multiplication factor to scattering cross section due to Gaussian-distributed angle of orientation ($\simeq 1$ for $s_\theta \gg \bar{\theta}+w_{1/2}$)
s_θ, s_L	standard deviation of angle of orientation or length
s	$s_L/\bar{L}$
$D(\theta)$	directivity pattern of scattering amplitude
$w_{1/2}$	half-width of $D(\theta)$ as measured between maximum response angle and e^{-1} point
θ	angle of orientation of cylinder: angle between direction of incident plane wave and the plane whose normal is the axis of the cylinder. For bent cylinders, the plane is positioned at the midpoint of the axis. $\theta=0$ is broadside incidence.
$\bar{\theta}$	average angle of orientation of cylinder
β	L/a (twice the aspect ratio)
ρ_c	radius of curvature of axis of uniformly bent cylinder

 0001-4966/93/94(6)/3463/10/$6.00

γ	position angle of bent cylinder
$\gamma_{\max}$	angle that subtends portion of bent cylinder between midpoint and end
TS	target strength
RTS	reduced target strength
W	probability distribution of angle or length
γ_κ	$(\kappa_2-\kappa_1)/\kappa_1$ (not to be confused with angular γ above)
κ	compressibility $[=(\rho c^2)^{-1}]$
γ_ρ	$(\rho_2-\rho_1)/\rho_1$ (not to be confused with angular γ above)
ρ	mass density
$\mathbf{k}_i$	wave vector of incident plane wave
$\mathbf{k}_s$	wave vector of scattered wave
μ	$\mathbf{k}_i-\mathbf{k}_s$
$\mu_{p=2}$	phase advance associated with crossing of caustics $[\simeq-(\pi/2)k_1a/(k_1a+0.4)]$, not to be confused with μ
$\mathbf{r}_0$	position vector of integration
v_0	integration volume
ϕ	$\cos^{-1}(\mathbf{k}_i\cdot\mathbf{k}_s/k_1^2)$
α_S,α_B, C_S,C_B	numerically determined coefficients
T_S,T_B	correction factors to account for tapering of cylinders
$\langle\cdots\rangle_\theta$	average over distribution of θ
$\langle\cdots\rangle_{\theta,L}$	average over distributions of both θ and L

INTRODUCTION

Mathematical descriptions of the scattering by individual zooplankton and subsequent comparison with laboratory data have demonstrated that the scattered level by an individual due to a single ping is strongly dependent upon size, shape, acoustic frequency, material properties (mass density and speed of sound contrast), and orientation.[1] There has been little information, however, involving the shape and orientation distributions of the animals. Estimates of average scattering cross section (averaged over size, shape, and orientation) are usually derived experimentally from scatter data by aggregations in a laboratory or natural ocean environment.[2,3] Very few predictions of averages exist using models and those that do involve numerical integration which do not conveniently illustrate the physics of the scattering process.[2,4,5]

While one may use echo data from aggregations of animals to estimate the average scattering cross section, the estimate is specific to that particular environment and does not necessarily lead to any insight or predictability as to the scattering by aggregations under other conditions where their behavior and hence orientation and shape distributions may be different. This article will explore the nature of the averaged echo from a theoretical standpoint so that data taken under one set of conditions can possibly be extrapolated to other conditions. As a minimum, both (1) the frequency/size dependence of the scattering by aggregations of animals and (2) the variability in the average echo due to changes in behavior will be better understood.

This article is organized as follows: (1) First, a ray model[1] that describes the scattering of sound by weakly scattering deformed cylinders near normal incidence and at one realization of angle of orientation and length is heuristically extended to approximately describe the backscatter by straight and bent cylinders as a function of angle of orientation for *all* angles. (This extension is only valid for the types of averages presented in this article, as the inaccuracies of the extension are negligible only after averaging.) (2) Those expressions are then averaged over Gaussian and uniform $(0-2\pi)$ distributions of orientation as well as a Gaussian distribution of length (with a relatively small standard deviation). (3) The expressions are directly compared with numerical simulations based on the Born approximation[6] which-does not have limitations with respect to angle of incidence, and two sets of data. (4) The usefulness and applicability of the research to the remote sensing of zooplankton are discussed.

I. ANGULAR DEPENDENCE OF SCATTERING

Because of the vast complexity of the problem of describing the scattering of sound by finite shaped bodies as a function of angle of incidence, a simplified ray version[1] of the approximate deformed cylinder solution[7] is used as a basis for the analytical expressions and heuristically adapted to the problem. The deformed cylinder solution has been shown to be reasonably accurate for angles of incidence near normal to the tangent of the lengthwise axis of elongated bodies with a high aspect ratio (i.e., high ratio of length to diameter). Typically that region is also where most of the acoustic energy is scattered by elongated zooplankton.[8] Near end-on incidence, the solution is inaccurate, although it does predict that the scattering levels near end-on are much lower than those observed at broadside. We proceed under the assumption that the averages over angle of orientation are relatively insensitive to the inaccuracies near end-on incidence. That is, as long as the approximate theory predicts a low value for near end-on, the inaccuracy of that value does not significantly affect the average over a wide range of angles because the echoes from near broadside will tend to dominate the average. Application of the formulas is best suited to the cases when broadside insonification occurs at least occasionally in a multiping sequence (a scenario that is quite typical when insonifying randomly oriented animals). The ray solution is also most accurate for values of $ka \gtrsim 0.1$. This latter restriction is certainly not limiting in this application since the animals are generally not detectable at or below those values of ka (Rayleigh scattering).

For the purposes of the mathematical averages, a Gaussian-shaped scatter directivity pattern is used in the scattering formulas. The function is mathematically convenient, and the "bell" portion of its curve broadly resembles the mainlobe of the scatter directivity pattern of the

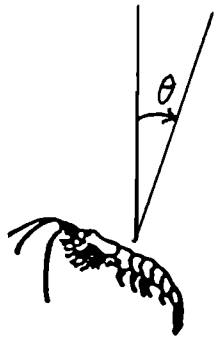

FIG. 1. An elongated zooplankton with a tilt angle of θ.

cylinders of interest (especially the straight cylinder). Its width and strength along the center axis are determined by a combination of simple geometrical arguments, estimates from the ray formulation, and comparison with numerical calculations. For near end-on incidence, the pattern predicts low levels as required.

The following definitions are useful in this analysis:

$$p_{\text{scat}}=P_0(e^{ikr}/r)f, \tag{1}$$

$$\sigma_{\text{bs}}=|f|^2 \quad \text{(backscatter direction)}, \tag{2}$$

$$\text{TS}=10\log\sigma_{\text{bs}}, \tag{3}$$

$$\text{RTS}=10\log(\sigma_{\text{bs}}/L^2), \tag{4}$$

where Eqs. (2)–(4) can also be expressed in terms of the cross section "σ" which is 4π times the above-defined (differential) backscattering cross section. The reduced target strength is a convenient dimensionless quantity used in displaying scattering levels by elongated bodies on a logarithmic scale.

The scattering amplitude and cross section for both the straight and bent cylinders are written in approximate (separable) form:

$$f\simeq D(\theta)f_0, \tag{5}$$

$$D(\theta)=e^{-\theta^2/(w_{1/2})^2}, \tag{6}$$

and

$$\sigma_{\text{bs}}\simeq D^2(\theta)(\sigma_{\text{bs}})_0, \tag{7a}$$

where

$$(\sigma_{\text{bs}})_0\equiv|f_0|^2, \tag{7b}$$

and θ is illustrated in Fig. 1.

The directional characteristics are shown to be contained solely in the $D(\theta)$ term which, in general, is not correct. However, for the cases in which the mainlobe of the scatter pattern is narrow, the strength of this lobe can be estimated with knowledge of the scattering amplitude at normal incidence (f_0). As stated before, the sidelobes of the pattern cannot be estimated by this method, but as long as $D(\theta)$ predicts small sidelobes that can be neglected in the averages over θ, it will be shown that such a formula can be used.

Simulations using the Born approximation in this section and in Sec. II test the accuracy of Eq. (5) and averages of Eq. (7a). The general equation describing the first-order Born approximation (or more precisely, the "distorted-wave" Born approximation where the wavenumber of the incident wave inside the body is determined by the material properties of the body) is given in Eq. 8.1.20 of Ref. 6 as

$$f=\frac{k^2}{4\pi}\int\int_{v_0}\int[\gamma_\kappa+\gamma_\rho\cos\phi]e^{i\mu\cdot r_0}\,dv_0, \tag{8}$$

where the notation of Ref. 6 was used in the right-hand side. (Note: The γ's appearing in this equation should not be confused with the angular γ's appearing elsewhere in this article. Also, the ϕ in this equation should not be confused with the ϕ in Ref. 1, which is the same as this ϕ only under certain conditions such as the backscattering geometry.) This equation is evaluated for all shapes described in this article and is valid for all angles of orientation. Only the first-order approximation is used since the calculations only involve weakly scattering fluidlike objects. All calculations in this article involving straight cylinders involved slightly tapered cylinders to round the ends hence reducing unrealistic end effects in the Born approximation solution such as due to flat ends (see caption to Fig. 2 and Table I for details). Although most bent cylinder calculations were relatively insensitive to tapering, the tapering was used in most cases for consistency with the straight cylinder calculations and to better match the tapered shape of the organisms.

A. Straight cylinder

A simplified approximate ray form of the backscattering amplitude due to a straight finite length cylinder (weakly scattering fluid) is given for values of $ka\gtrsim 0.1$ as[1]

$$f\simeq(-i/2\sqrt{\pi})e^{i\pi/4}e^{-i2k_1a\cos\theta}\times L\sqrt{k_1a\cos\theta}\,\mathscr{R}_{12}(\sin\Delta/\Delta)I, \tag{9}$$

where

$$I=1-T_{12}T_{21}e^{i4k_2a\cos\theta}e^{i\mu_{p=2}(k_1a)}. \tag{10}$$

Since f varies slowly with θ near-normal incidence (provided values of ka are away from nulls in the f vs ka curve), the directivity pattern is given approximately as $\sin\Delta/\Delta$ and

$$f_0=(-i/2\sqrt{\pi})e^{i\pi/4}e^{-i2k_1a}L\sqrt{k_1a}\,\mathscr{R}_{12}I_0, \tag{11}$$

where I_0 is I evaluated for $\theta=0$.

In order to replace the sinc function directivity pattern by a Gaussian function, the following is observed:

$$\sin\Delta/\Delta\simeq 1-\tfrac{1}{6}(kL)^2\theta^2 \quad (kL\sin\theta\ll 1,\quad \theta\ll 1). \tag{12}$$

Since this has the same form as the first two terms of a Taylor expansion of an exponential function, the directivity function is written as

$$D(\theta)\sim e^{-\alpha_S(kL)^2\theta^2}, \tag{13}$$

where

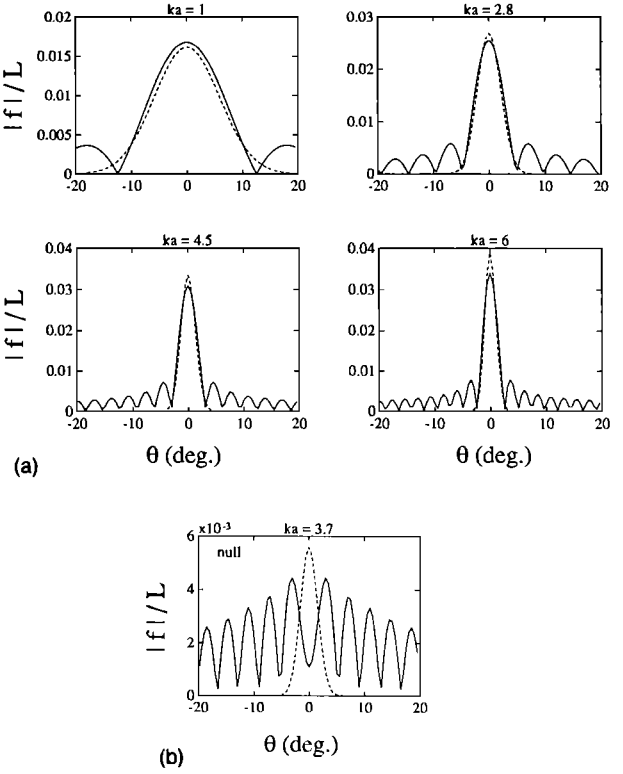

FIG. 2. (a) Comparison between the Born approximation solution for a straight cylinder (solid line) and a (dashed) Gaussian curve [Eq. (13)]. The parameters $\alpha_s(=0.2)$ in the exponent of the Gaussian as well as a multiplicative factor C_s were chosen by visual inspection so that there would be a good fit between the width and height, respectively, of the mainlobes of the two curves. The tapering function, $a(z) = \sqrt{1-[z/(L/2)]^{10}}$, where z is the position along the axis, was chosen to round the ends of the cylinder to reduce unrealistic scattering by the sharp edges. The radius of the cylinder is essentially constant over about 60% of the length of the cylinder before it tapers to zero at the ends. Note that the cylindrical radius averaged along the axis is very close to the maximum value of the radius at the midsection. For simplicity, the "a" in ka in all simulations represents the value of a at the midsection. The amplitude of the Gaussian is weighted by the multiplication of three factors: T_S and C_S (see Table I) and the straight untapered cylinder ray solution (normal incidence). The value of ka was chosen so that the scattering was near a maximum on the scatter versus ka curve. (b) Similar to (a) but illustrating poor fit when ka is near a null. The values $(g,h)=(1.0357, 1.0279)$ in both (a) and (b).

$$w_{1/2}=(\sqrt{\alpha_s}kL)^{-1} \text{ was used in Eq. (6).} \qquad (14)$$

and α_S is a numerically determined coefficient so that the main lobe of the Gaussian directivity pattern has a best fit with the mainlobe of the sinc function.

The usefulness of the Gaussian function in this application is shown in Fig. 2 where the mainlobes of both the Gaussian function and Born approximation solution compare reasonably well (provided the value of ka is away from a null). There is very little correspondence between the two curves for higher angles of incidence except for the fact that they both describe decreasing trends of scattering versus angle. As previously emphasized, the mainlobe is the most important component to model while inaccuracies in the high angle region are much less important, if not negligible, once averaging is performed.

TABLE I. Values of A_{ij} for all four combinations of cylinder shape and distribution of angle of orientation θ. Here, T, C, and α are correction factors for the straight (subscript S) and bent (subscript B) cylinders. The straight cylinders were slightly tapered by the function $a(z) = \sqrt{1-[z/(L/2)]^{10}}$ where z is the position along the axis to round the ends of the cylinder. This tapering was performed to be consistent with the Born approximation calculations, all of which involved the same tapering (straight *and* bent cylinders). The factors T_S and T_B, derivable from the deformed cylinder formulations, are used to correct scattering levels due to any tapering of the cylinder. In our analysis, the straight cylinder levels were affected the most by tapering resulting in the range $0<T_S<1$, and T_B is fixed at unity since we observed little influence of the tapering on the bent cylinder calculations. Also, α_S, α_B, C_S, and C_B are empirically determined coefficients for best fits to the numerical simulations of backscatter versus angle of orientation based on the Born approximation. Note also that C_S, C_B, and $\mathcal{S}_\theta$ are near unity. Specifically, $(\alpha_S,\alpha_B)\sim(0.2,0.8)$; $(C_S,C_B)\sim(0.9,1.2)$ (all numerically determined correction factors), $T_S=\{1-[(n-\frac{1}{4})\pi/2k_1a]^2\}^{1/m}$, where $m=10$ and n is within the bounds $(2k_1a/\pi)-\frac{3}{4}\leqslant n\leqslant(2k_1a/\pi)+\frac{1}{4}$ and can be determined by minimizing $1-[(n-\frac{1}{4})\pi/2k_1a]^2$, and $T_B=1$.

A_{ij}	Gaussian distributed orientation	Uniformly distributed orientation
Straight cylinder	$\dfrac{T_S^2C_S^2\mathcal{S}_\theta}{8\pi\sqrt{\alpha_S s_\theta}}$	$\dfrac{T_S^2C_S^2}{4\pi\sqrt{2\pi}\sqrt{\alpha_S}}$
Bent cylinder	$\dfrac{T_B^2C_B^2\mathcal{S}_\theta}{16\sqrt{\alpha_B s_\theta}}$	$\dfrac{T_B^2C_B^2}{8\sqrt{2\pi}\sqrt{\alpha_B}}$

B. Bent cylinder

A simplified ray form of the backscattering amplitude due to a bent finite length cylinder (weakly scattering fluid) is given for values of $ka\gtrsim 0.02$ at broadside incidence as[1]:

$$f_0\simeq(1/2)\sqrt{\rho_c a}\mathcal{R}_{12}e^{-i2k_1a}I_0, \qquad (15)$$

where I_0 is defined after Eq. (11). Equation (15) involves scattering where the cylinder is bent symmetrically away from the sonar.

There is no form of Eq. (15) that conveniently shows directivity of the scattering, hence the directivity must be derived purely from geometrical arguments. We assume that there is only significant return from the cylinder when the direction of the incident field is normal to some point along the axis of the body (i.e., angles more toward broadside incidence). Once the cylinder is oriented more toward end-on incidence so that at *no* point is the direction of the incident field normal to the axis, the return would dramatically decay with increasing angle. The directivity is therefore written with a Gaussian function whose e^{-1} level corresponds to near the point at which the direction of the incident field is normal to the tangent to the axis at the *end* of the cylinder (i.e., when $\theta=\gamma_{\max}$):

$$D(\theta)\simeq e^{-\alpha_B(\theta/\gamma_{\max})^2}, \qquad (16)$$

or equivalently

$$D(\theta)\simeq e^{-\alpha_B(2\theta\rho_c/L)^2}, \qquad (17)$$

where

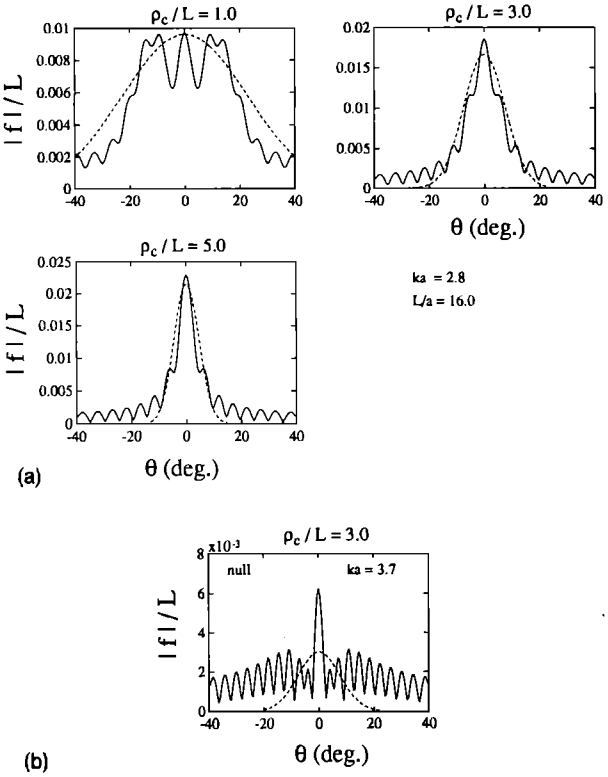

FIG. 3. (a) Comparison between the directional characteristics of the backscattering by a bent cylinder as determined numerically from the Born approximation solution (solid line) and a (dashed) Gaussian curve [Eq. (17)]. The ends of the cylinders in the Born solution are rounded as described in Fig. 2 caption although there was no need to correct for tapering in the Gaussian curve (Tapering apparently has little affect on the bent cylinder calculations hence, although it was included in the Born calculations; the "correction" factor to the Gaussian curve was unity.) As in Fig. 2, the parameters $\alpha_B(=0.8)$ and a multiplicative factor C_B were chosen by visual inspection so that there would be a good fit between the mainlobes and height, respectively, of the two curves. Three bends are investigated: $\rho_c/L=1,3,5$. The amplitude of the Gaussian was weighted by the product of the bent cylinder ray solution and a visually determined empirical factor $C_B(=1.2)$. The value of ka was chosen so that the scattering was near a maximum on the scatter versus ka curve. (b) Similar to (a) but illustrating poor fit when ka is near a null. $(g,h)=(1.0357,1.0279)$ and $L/a=16$ in both (a) and (b).

$w_{1/2}=\gamma_{\max}/\sqrt{\alpha_B}=L/(2\rho_c\sqrt{\alpha_B})$ was used in Eq. (6). (18)

Hence, D is near unity when the direction of the incident field is normal to some point on the axis within the cylinder and D is exponentially small when the cylinder is tilted so far that at no point is the direction normal. The term α_B is determined numerically so that the mainlobe of the Gaussian function best fits the corresponding lobe calculated from the Born approximation solution.

Application of the Gaussian beampattern to the scattering by bent cylinders is illustrated in Fig. 3. As in the corresponding plot for the straight cylinders in Fig. 2, the width of the mainlobe is reasonably described by the Gaussian function (with the same provision that the value of ka is away from a null) while the low-amplitude structure in the region of high-angle scattering is not. Note that in contrast to the straight cylinder, the mainlobe calculated from the Born approximation solution is somewhat oscillatory. This is largely due to the fact that the number of Fresnel zones that occupy the cylinder vary with orientation angle. There are also some small effects due to the scattering from the ends.

II. AVERAGES

A. Distributions

Averaging the echoes over a range of orientations requires knowledge of the orientation distribution of the objects. There is very little information regarding the angular distribution of zooplankton. To the authors' knowledge, only means and standard deviations of angle have been reported.[9–13] Distributions of angle and related averages have been studied to a much greater extent in the field of fisheries acoustics. It has been observed that the angle of orientation or "tilt" angle of fish is generally Gaussian in nature.[14–16] Averages of cross sections using such distributions have compared well with data.[17–19] Because of the success of using the Gaussian function to describe fish behavior and the mathematical convenience of using such a function, the following Gaussian function is used to describe the orientation distribution of zooplankton under certain conditions:

$$W(\theta)=(1/\sqrt{2\pi}s_\theta)e^{-(\theta-\bar{\theta})^2/2s_\theta^2}. \quad (19)$$

It is anticipated that this function is most applicable when the animals demonstrate a preferred orientation direction $\bar{\theta}$ about which the orientation is normally distributed. (A candidate for such a scenario would be use of a down-looking sonar to examine zooplankton that are swimming in a horizontal or near-horizontal orientation.)

If, in contrast to the above, the animals are swimming chaotically, the uniform distribution may be more appropriate:

$$W(\theta)=1/2\pi, \quad (20)$$

in which case the animals have no preferred orientation and θ is distributed uniformly from 0 to 2π. This distribution may also possibly apply for the case of a side-looking sonar where θ would represent the angle of orientation in the horizontal plane. In this latter case, θ has a great likelihood of being uniformly distributed.

Information on the distribution of lengths of zooplankton is also scarce although Ref. 20 shows that the lengths of one species follows the Gaussian. Because of the success of this function to describe fish lengths and its mathematical convenience, we use the Gaussian to describe the distribution of lengths:

$$W(L)=(1/\sqrt{2\pi}s_L)e^{-(L-\bar{L})^2/2s_L^2}. \quad (21)$$

This function may only apply to certain populations of animals whose size distribution is Gaussian. The following general scattering formulas can take into account *any* size distribution. Also, the specific formulas given at the end of this article that involve narrow Gaussian distributions of size can apply to each size class (or subset of size) of a more general distribution.

Finally, integrals involving the above Gaussian distributions of both angle and length, if not properly truncated,

involve unrealistic values of angle and length. For example, one can theoretically extend the range of angles of orientation beyond the range of $0-2\pi$. Also the lengths can span the $-\infty$ to $+\infty$ range. In practice, when one performs the integrals numerically the values of angle and length are restricted to realistic values as well as not being beyond 2 standard deviations (s.d.) from the mean value. Conversely, when one performs the integrals analytically, the limits in both cases are extended to $\pm\infty$ for convenience. Comparison with numerical integration indicates no significant difference between the two methods because of the exponentially small values of the integrand at the extreme limits.

B. General formulas

Since echoes from zooplankton in aggregations tend to add incoherently at sufficiently high acoustic frequencies, the cross sections are averaged. Hence, the average cross sections are calculated according to the following formulas:

$$\langle\sigma_{bs}\rangle_\theta = \int W(\theta)\sigma_{bs}\, d\theta \tag{22}$$

and

$$\langle\sigma_{bs}\rangle_{\theta,L} = \int\int W(\theta)W(L)\sigma_{bs} dL\, d\theta, \tag{23}$$

where both the averages over angle only and over angle and length are given. Using Eqs. (6), (7a), (19), and (22), the following general formula is derived for both straight and bent cylinders, assuming that the distribution of angles is Gaussian and $s_\theta \gtrsim \bar{\theta}+w_{1/2}$:

$$\langle\sigma_{bs}\rangle_\theta \simeq (\sqrt{2\pi}s_\theta)^{-1}(\sigma_{bs})_0 \int_{-\infty}^{\infty} e^{-(\theta-\bar{\theta})^2/2s_\theta^2} e^{-2\theta^2/(w_{1/2})^2}\, d\theta \tag{24a}$$

$$= (\sigma_{bs})_0 (w_{1/2}/2s_\theta)\mathscr{S}_\theta \text{ (bent/straight cylinders, Gaussian tilt angle, } s_\theta \gtrsim \bar{\theta}+w_{1/2}), \tag{24b}$$

where $(\sigma_{bs})_0$ is the scattering cross section for *either* the straight or bent cylinder and is not restricted to any particular boundary condition. The restriction $s_\theta \gtrsim \bar{\theta}+w_{1/2}$ was imposed for reasons discussed earlier in the text: for the Gaussian shaped scatter pattern $D(\theta)$ to be valid, the mainlobe of the scatter pattern of the animal must be the main contributor to the integral, hence representing the dominant source of backscatter energy (as opposed to sidelobes). The width of the distribution of tilt angle must then be large enough so that angles near broadside angle occur a substantial percentage of the time [i.e., $W(\theta)$ is still near its maximum value when the animal is oriented broadside]. The limits of the $\int_{-\pi}^{\pi}$ integral are extended to $\pm\infty$ for mathematical convenience since the integrand is exponentially small beyond 2 s.d. from the mean.

Under the restriction $s_\theta \gtrsim \bar{\theta}+w_{1/2}$, the function

$$\mathscr{S}_\theta = \frac{2s_\theta}{w_{1/2}}\left(1+\frac{4s_\theta^2}{(w_{1/2})^2}\right)^{-1/2} \times \exp\left\{-\frac{\bar{\theta}^2}{2s_\theta^2}\left[1-\left(1+\frac{4s_\theta^2}{(w_{1/2})^2}\right)^{-1}\right]\right\} \tag{25}$$

is only mildly dependent upon s_θ. For $s_\theta \gg \bar{\theta}+w_{1/2}$, $\mathscr{S}_\theta \to 1$.

For the case of uniformly distributed orientation angles, the average cross section is calculated by use of Eqs. (6), (7a), (20), and (22):

$$\langle\sigma_{bs}\rangle_\theta \simeq \pi^{-1}(\sigma_{bs})_0 \int_{-\infty}^{\infty} e^{-2\theta^2/(w_{1/2})^2}\, d\theta \tag{26}$$

$$= (2\pi)^{-1/2}(\sigma_{bs})_0 w_{1/2} \text{ (bent/straight cylinders, uniform tilt angle),} \tag{27}$$

where, again, $(\sigma_{bs})_0$ can be the scattering cross section for *either* the straight or the bent cylinder and is not restricted to any particular boundary condition. As in Eq. (24), the limits of the $\int_{-\pi}^{\pi}$ integral are extended to $\pm\infty$ for mathematical convenience at a negligible loss of accuracy. There was an extra factor of two incorporated in Eq. (26) due to the (near) symmetry of the scattering at $\theta=\pi$. [This was incorporated heuristically since $D(\theta)$ does not reflect the symmetry.] It was not necessary to take into account the symmetry in Eq. (24) since the animals spent only a negligible fraction of time in that orientation due to the Gaussian tilt distribution.

C. Weak scatterer (fluidlike zooplankton) formulas

For the weak scatterer case, $(\sigma_{bs})_0$ in Sec. II B can be replaced by the ray-based scattering equations to yield the following compact formulas that are valid for $ka \gtrsim 0.1$:

$$\langle\sigma_{bs}\rangle_\theta = A_{ij}\mathscr{R}_{12}^2 |I_0|^2 aL, \tag{28}$$

$$\langle\sigma_{bs}\rangle_\theta / L^2 = A_{ij}\mathscr{R}_{12}^2 |I_0|^2 \beta^{-1}, \tag{29}$$

and

$$\langle\sigma_{bs}\rangle_{\theta,L} / \bar{L}^2 = A_{ij}\mathscr{R}_{12}^2 \langle |I_0|^2\rangle_L \beta^{-1}. \tag{30}$$

Each formula represents all combinations of straight and bent cylinders with Gaussian and uniform distributions of tilt angle. The differences in shape and distribution are reflected in A_{ij} (Table I). Equations (28) and (29) involve averages over angle only while Eq. (30) involves an average over a narrow distribution of length as well. Equations (29) and (30) show the average cross section to be normalized by the square of the length (a convenient dimensionless form) with the aspect ratio $\beta/2 \equiv L/2a$ incorporated. (Animal shapes tend to remain constant over a range of sizes making the aspect ratio a useful parameter.) The average $\langle |I_0|^2\rangle_L = 2\{1-\exp[-8(k\bar{a}s)^2]\cos(4k\bar{a}+\mu_{p=2})\}$ was evaluated assuming a narrow ($s \sim 10\%$) length distribution.

Some of the approximate weak-scatterer formulas presented above are studied over a range of conditions by comparisons with Monte-Carlo-averaged Born approximation solutions (Figs. 4 and 5). Illustrated are (1) the near independence of the averages with respect to degree of

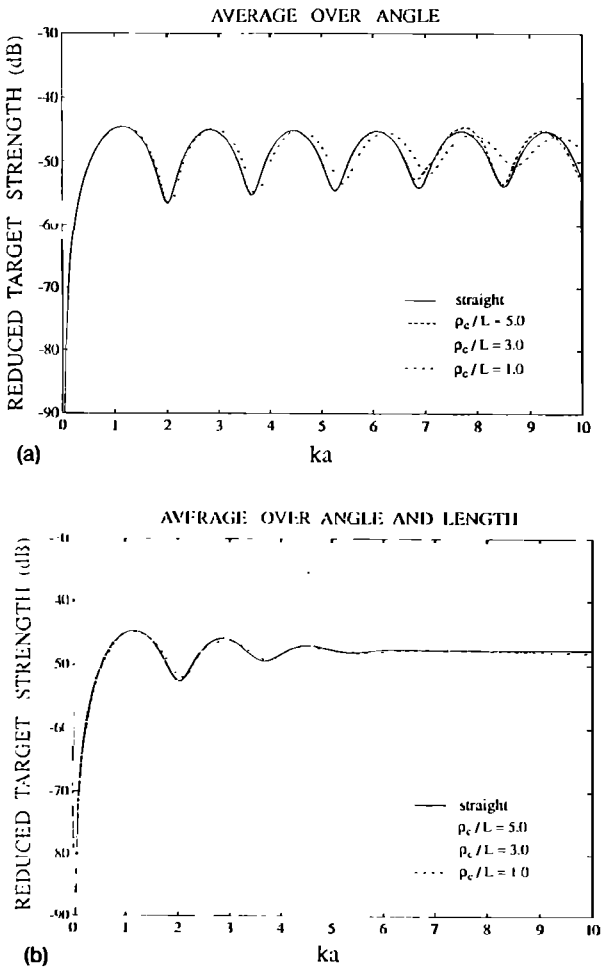

FIG. 4. Reduced target strength based on average backscattering cross section versus ka for finite cylinders of various bends. All calculations are based on the Born approximation and involve cylinders with rounded ends (see Fig. 2 caption). Same values of g, h, and L/a as in Fig. 3 caption. (a) Averaging over angle only [$N(0°,40°)$]. (b) Averaging over angle and length [$N(0°,40°)$ and s.d.$=0.1\ \bar{L}$]. All calculations indicate that the average cross sections are virtually independent of the bend of the cylinder provided that $\rho_c/L \gtrsim 2$ and that the s.d. of the angular distribution is much greater than the sum of the mean angle and half-width of the mainlobe of the scatter pattern of the target. In (b), the cross section is shown to also be independent of ka for high ka once the average is taken over length.

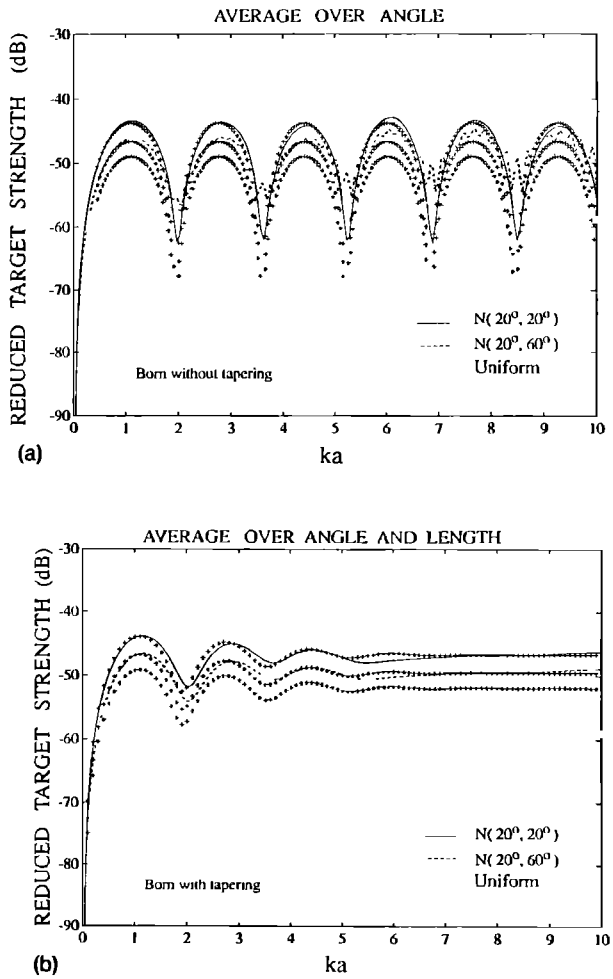

FIG. 5. Reduced target strength based on average backscattering cross section versus ka for bent cylinders of various orientation parameters. The curvature is the same for all cylinders ($\rho_c/L=3.0$). Same values of g, h, and L/a as in Fig. 3 caption. Averaging is over angle only in (a) and both angle and length (s.d.$=0.1\ \bar{L}$) in (b). The solid and broken lines are based on Monte Carlo simulations of the Born approximation solution [untapered in (a) and rounded ends in (b)] while the points indicated by the "+" characters are based directly on the simple analytical formulas given in Eqs. (29) and (30) with no tapering in either (a) or (b). The cylinders were not tapered in the Born approximation in (a) for direct comparison of the deep nulls predicted by Eq. (29) and the Born approximation (the tapering results in rounding them). Once averages over length are performed, the nulls are further rounded making the difference between the tapered and untapered solution small. The approximate formulas are shown to follow the structure and overall levels of the Born approximation solution.

bend of the cylinder, (2) the rounding or partial "filling in" of the modal nulls at $ka=2$, 3.7, 5.2, etc., (3) independence with respect to ka for $ka \gg 1$ once the echoes are averaged over both angle and length, and (4) the reasonable fit between the Born approximation solution and the simplified ray-based solution.

III. ZOOPLANKTON BACKSCATTER DATA

We present two sets of data to compare with the approximate formulas derived in this article: The first, published by Foote *et al.*,[21] involving hundreds of krill (*Euphausia superba*, a shrimplike zooplankton) encaged in the ocean and the second collected at the Woods Hole Oceanographic Institution (WHOI) by these authors involving several sets of tethered aggregations of decapod shrimp (*Palaemonetes vulgaris*) totalling up to 12 animals each.

The krill experiment was performed in the harbor of Stromness on South Georgia in January and February, 1988. For each experiment, hundreds of encaged animals were insonified with 38- and 120-kHz echo sounders. The TS values extracted from the data were derived from measurements on the aggregations of echo energy (or volume scattering strength), averaged over many pings. Since the animals were allowed to swim freely within the cage, moving from ping to ping, the average energy is related to the cross section averaged over angle of orientation. Measurements of length distribution and speed of sound and density contrasts of the animals at the time of the experiments allowed meaningful comparison between the data and scattering models in Refs. 2, 5, and 21.

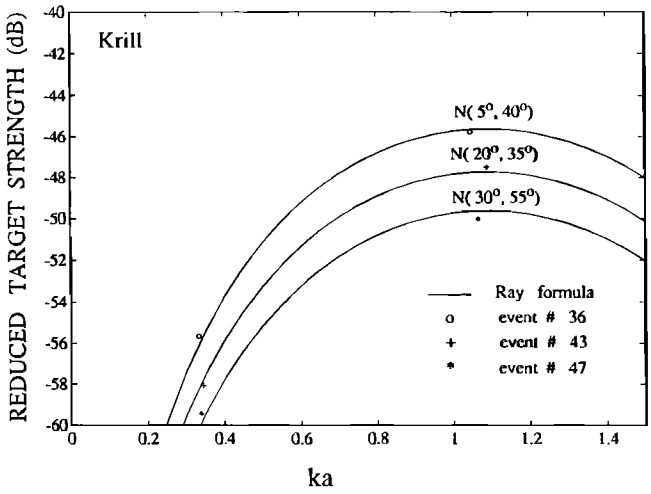

FIG. 6. Comparison between the 38/120 kHz data pairs of average backscattering from aggregations of krill as measured in several independent experiments. Superimposed is the reduced target strength based directly on the simple formula for average backscattering cross section from Eq. (30) (bent cylinder, Gaussian distributed tilt angle) for several mean and s.d. of angle of orientation. (Data from Foote *et al.*[21]) Same values of g, h, L/a, and ρ_c/L as in Fig. 5. The variability in levels from experiment to experiment suggests possible changes in behavior in the animals.[5] The "a" value for each data point is based on the average L/a value and measured length L.

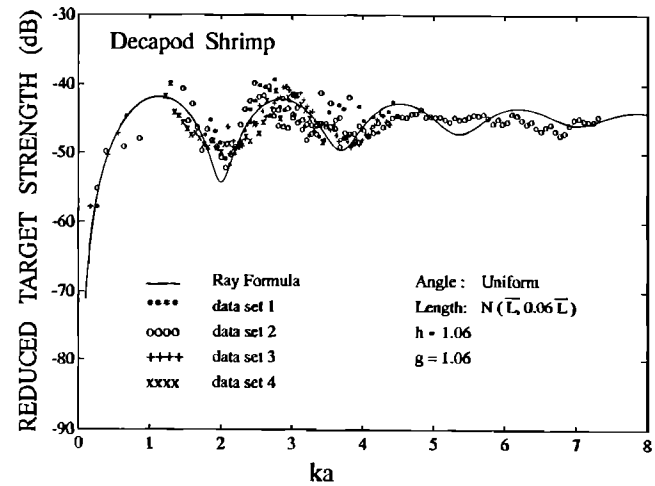

FIG. 7. Comparison between backscatter data collected at WHOI over a wide range of frequencies (50 kHz–1.2 MHz) and predictions directly from Eq. (30) (bent cylinder, uniformly distributed tilt angle) for four sets of aggregations of decapod shrimp. Same value of L/a as in Fig. 5 (ρ_c/L was not needed in this equation; g and h, material properties that were not measured in this experiment, were varied to adjust the overall level of the curve). The "a" value for each data point is the equivalent cylindrical radius $\bar{a}$ given in Table II. The value s=0.06.

Some of the data presented in Refs. 2 and 21 are given in Fig. 6 for comparison with the formulas derived in this article. Three pairs of points (one pair per experiment) are plotted along with simple ray-based calculations [from Eq. (30), bent cylinder/Gaussian distributed tilt angle] of average cross section normalized by the square of the length. Each pair of points corresponds to measurements at two different acoustic frequencies. A different set of animals was used to produce each pair. The mean and standard deviation of angle of orientation in the calculations were adjusted to provide a best fit to the data.

The experiment performed at WHOI (summer, 1992) involved aggregations of far fewer animals, but with a wider range of acoustic frequencies, 50 kHz to 1.2 MHz. A total of four experiments were conducted, each involving an aggregation of 6–12 animals. The sizes of the animals in each aggregation were chosen so that they would lie within approximately 10% of the ~2-cm-mean lengths (Table II). The live animals (not anesthetized) were tethered by (acoustically transparent) human hair in such a way that they each could move within a short range (of the order cm's) while at the same time be confined within the acoustic beam. (All beams had approximately a 20-cm-diam "footprint" at the 1.2-m range.) All animals were tied along a strand(s) of vertical hair that was left slightly loose to allow movement (one strand for experiments 1–3, two parallel strands for experiment 4). The transducers were aimed horizontally. Visual observations throughout the experiments verified that there was movement of animals. The deviations of the positions of the animals from a straight line were enough so that there would be incoherent addition of the echoes from the individuals. The animals tended to be "aimed" in different directions. As the array of animals swam around in small circles, the echo noticeably varied from ping to ping. The combination of visual observations and observation of the variability of the echoes suggests statistical independence of the echoes—a condition required for averaging the energies of the echoes.

TABLE II. Summary of measured parameters of decapod shrimp used in experiments. Here, n is the total number of animals, $\bar{L}$ is the mean total length measured from anterior of the eye to the tip of the telson, s_L is the s.d. of L, $\bar{a}_t$, and $\bar{a}$ are average radius of thorax and average equivalent cylindrical radius of entire body as calculated from its volume, respectively, and w is the average wet weight.

Data set No.	n	$\bar{L}$ (mm)	s_L (mm)	$\bar{a}_t$ (mm)	$\bar{a}$ (mm)	w (mg)
1	6	21.2	1.2	1.6	1.3	116.1
2	6	21.8	1.2	1.7	1.4	122.8
3	7	15.7	0.9	1.1	0.9	37.6
4	12	16.0	1.0	1.3	1.1	55.7

The lower frequency transducers (50, 75, 120, and 165 kHz) transmitted gated sine waves (i.e., essentially single frequency signals) while the higher frequency transducers (center frequencies of 500 kHz and 1 MHz) transmitted chirp signals with frequency spectra covering the ranges of, approximately, 250–750 kHz and 500 kHz–1.2 MHz, respectively. Because of the large number of transducers (one transmit/receive pair per frequency), only one pair at a time was in the water. At least 100 pings per transducer pair were recorded. Due to logistical difficulties of mounting and calibrating each transducer pair only a subset of transducer pairs was used in each experiment. Details of the calibrations of the broadband transducers are given in Ref. 22 while the single frequency transducers were calibrated in a similar manner.

All data were combined for the dimensionless plot of reduced target strength versus ka and compared with the

approximate ray solution from Eq. (30) (bent cylinder, uniformly distributed angles) (Fig. 7). The data are shown to exhibit much of the trend and structure as that of the predictions: The data increase rapidly and monotonically in the $0.3 < ka < 0.7$ region (Rayleigh scattering) while eventually leveling off to a more-or-less constant level in the $ka \sim 5$ region (geometric scattering). Both the data and predictions show a strong dip near $ka = 2$ and a weaker, yet noticeable one near $ka = 3.8$. For values of $ka > 4$ both exhibit smaller dips and peaks also, although there is less correlation between the predicted and observed locations of that structure.

IV. DISCUSSION

An important theoretical result obtained in this article is the fact that for a sufficiently wide range of angle of orientation (i.e., the s.d. is much larger than the sum of the mean angle and half-width of the mainlobe of the scatter pattern), the average backscattering cross section is essentially independent of degree of bend of the cylinder for $\rho_c/L \gtrsim 2$ [Eqs. (28)–(30), Fig. 4]. The independence is due to the law of conservation of energy. The more the object is bent, the lower the level of energy scattered in the backward direction. However, the energy becomes increasingly diffuse over a broader range of directions as the object is bent. Thus integration over a range of angles that contains the mainlobe of scattering is more-or-less constant due to the offsetting effects. For small ranges of angle of orientation, there are frequency and shape dependences as the average involves only a portion of the mainlobe.

The independence of the average energy with respect to bend is important in remote sensing applications. As demonstrated in Ref. 7, one realization of the scattering by an individual is strongly dependent upon the bend. Hence, when one is detecting individuals in the field environment, the echo can vary dramatically due to variations in shape of the animal. Once the echo is averaged over many realizations, however, the resultant energy is essentially independent of the bend distribution, hence eliminating the need for that parameter in the interpretation of the data.

The expressions in Eqs. (28)–(30) also show that the average cross section is strongly dependent upon the size of the object (cylindrical radius and length) as well as its s.d. of angle of orientation. The dependence upon the angle parameters is illustrated in Fig. 5 where the distribution of angle is varied. The levels of each curve are generally predicted by the bent cylinder equation in Eqs. (29) and (30), especially near the local maxima. As one would expect, the deep nulls in the scatter versus ka plots are at least partially "smoothed" out once averages over length are performed [Eq. (30), Fig. 5(b)] resulting in an independence of both shape and frequency in the limit of high ka.

Both relative levels and structure of the zooplankton backscatter data are consistent with the theoretical predictions. While the Foote *et al.*[21] data only involve two frequencies, the general upward trend of the data with respect to frequency is predicted by the theory. The WHOI data covers a large range of frequencies and shows significant structure. The data are shown to increase in the Rayleigh ($ka < 1$) region and more or less level off for values above $ka = 1$ (geometric region). All four sets of (WHOI) data show dips in regions similar to those predicted by the theory. There is especially good agreement near the $ka = 2$ and $ka = 3.8$ dips both with respect to position and relative level. Note that, although the four sets involve four different aggregations of animals of different mean lengths, all data are reasonably consistent with each other on this dimensionless scale indicating the quality and consistency of the experiment.

It is also very important to observe that the data appear to become independent of frequency for high ka, as predicted by theory. This independence of the aggregation echo should be compared with the observation of a general upward trend in laboratory data involving individuals near broadside incidence.[23,24] Such a trend may be due to natural differences in the experiments since only echoes from near-normal incidence were recorded with the individuals as opposed to the aggregation echo which involved scattering from all angles of incidence. It is possible that there are conditions in the natural environment and/or echo sounder configurations where one set of data may be more applicable than the other. For example, if the echo sounder is aimed in the vertical direction and the animals are swimming so that they are all near broadside to the sounder, then the data from Refs. 23 and 24 may apply. If, however, the animals are swimming chaotically in all directions with the echo sounder aimed vertically, or if the sounder is aimed horizontally and the animals are hovering or swimming chaotically, the WHOI aggregation data may be more applicable.

Finally, as discussed in Ref. 7, certain classes of animals that are elongated can be modeled by use of a cylinderlike shape as opposed to other animals where the sphere may be more appropriate (Ref. 25). The curve in Fig. 7 broadly resembles that of the sphere scattering amplitude in that it rises rapidly for $ka < 1$ and levels off above $ka = 1$. However, in Fig. 7 the "a" in ka is the cylindrical radius based on the cylindrical cross section of the animals. If one were to plot the data against a sphere model and the "a" is now the *spherical* radius, the equivalent spherical radius of the animals would have had to be computed based on the animals' volume. The result would have shifted the data to the right by a factor of about 2 on this plot while the corresponding sphere-scattering curve would have remained in the same position [see Fig. 7(c) of Ref. 22]. Hence, the data would have been grossly misaligned with the sphere predictions. Also, there is potential for the general levels of the sphere predictions to be different from the scattering data due to the lack of behavior parameters in the sphere model. Thus it is apparent that these particular animals behave acoustically as finite cylinders (either straight or bent).

V. CONCLUSIONS

Formulas have been derived that estimate the backscattering cross section of finite cylinders averaged over angle of orientation and length. Comparisons have been made with simulations and data involving elongated zoo-

plankton. The analysis shows that (1) under certain conditions, the average cross sections are independent of the bend of the cylinder, (2) under all conditions the averages depend upon the s.d. of angle of orientation, and (3) The predictions and backscatter data, while leveling off with respect to frequency at high frequencies contain significant structure in the form of 5- to 8-dB dips.

These results are important to the bioacoustic scientific community. Since precise bend of free-swimming zooplankton is generally not known and since the (unaveraged) backscattering cross section is dramatically dependent upon bend, it is extremely useful to know that the bend is much less a factor once averaging over an aggregation of animals is performed. With this factor reduced or eliminated, it becomes more possible to extract other information from the data. For example, for a given aggregation of zooplankton, the orientation behavior of the animals can possibly be inferred from data consisting of repeated measurements and running averages of the echo energy.[5]

Finally, the structure in the scattering versus ka plots remains significant in spite of averages over length and orientation. Hence the dips near $ka=2$ and $ka=3.8$ are to be expected and strategies to account for their effects need to be developed. Specifically, the nonlinear nature of the data in Fig. 7 illustrates the need for models more sophisticated than size cross-section linear regression relationships. Holliday, Pieper, and collaborators have been successful in applying a nonlinear scattering model (truncated fluid sphere model) to multifrequency data from (nearly spherical) zooplankton smaller than about 10 mm.[25] Their inversion of the data produced size distributions of the animals. Thus these authors recommend similar inversions of multifrequency data from the elongated zooplankton using nonlinear models such as the cylinder model presented in this article.

ACKNOWLEDGMENTS

The authors would like to thank the following people of the Woods Hole Oceanographic Institution (WHOI), Woods Hole, MA: Shirley Bowman for preparing the manuscript to this article, Matt Johnson and Bob Eastwood for assisting in the experiments, and Paul Boutin, John Kemp, and John Bouthillette for designing and constructing much of the mechanical apparatus involved. This research was inspired, in part, by conversations between two of the authors (TKS and DC) and Dr. Kenneth G. Foote of the Institute of Marine Research, Bergen, Norway, during Dr. Foote's visit to the Institution, summer 1991. Dr. Foote also provided useful suggestions on the manuscript. This research was supported by the Oceanic Biology and Ocean Acoustics Programs of the U.S. Office of Naval Research Grant No. N00014-89-J-1729 and the Office of Naval Technology (through the U.S. Naval Undersea Warfare Center, Newport, Contract No. N66604-91-C-5401). This is Contribution Nos. 8178 and 549 for the Woods Hole Oceanographic Institution and Geophysical and Polar Research Center, University of Wisconsin—Madison, respectively.

[1] T. K. Stanton, C. S. Clay, and D. Chu, "Ray representation of sound scattering by weakly scattering deformed fluid cylinders: Simple physics and application to zooplankton," J. Acoust. Soc. Am. **94**, 3454–3462 (1993).

[2] K. G. Foote, D. Chu, and T. K. Stanton, "Status of krill target strength," CCAMLR Select. Sci. Papers (in press).

[3] For a list of references involving estimates of average target strength from measurements of volume scattering strength of aggregations of krill, see Ref. 2.

[4] N. A. Cochrane, D. Sameoto, A. W. Herman, and J. Neilson, "Multiple-frequency acoustic backscattering and zooplankton aggregations in the inner Scotian Shelf basins," Can. J. Fish. Aquat. Sci. **48**, 340–355 (1991).

[5] D. Chu, K. G. Foote, and T. K. Stanton, "Further analysis of target strength measurements of Antarctic krill at 38 kHz and 120 kHz: Comparison with deformed cylinder model and inference of orientation distribution," J. Acoust. Soc. Am. **93**, 2985–2988 (1993).

[6] P. M. Morse and K. U. Ingard, *Theoretical Acoustics* (Princeton U.P., Princeton, N.J., 1968), Chap. 8.

[7] T. K. Stanton, "Sound scattering by cylinders of finite length. III. Deformed cylinders," J. Acoust. Soc. Am. **86**, 691–705 (1989).

[8] C. F. Greenlaw, (unpublished data).

[9] Y. Endo, "Swim angles of *Euphausia pacifica*," Proc. NIPR Symp. Polar Biol., **2**, 219 (1989).

[10] U. Kils, "Preliminary data on volume, density and cross section area of Antarctic krill, *Euphausia superba*," Meeresforsch **27**, 207–209 (1979).

[11] U. Kils, "The swimming behavior, swimming performance and energy balance of Antarctic krill, *Euphausia superba*," BIOMASS Sci. Ser. **3**, 122 (1981).

[12] A. Kristensen and J. Dalen, "Acoustic estimation of size distribution and abundance of zooplankton," J. Acoust. Soc. Am. **80**, 601–611 (1986).

[13] D. D. Sameoto, "Quantitative measurements of euphausiids using a 120-kHz sounder and their *in situ* orientation," Can. J. Fish. Aquat. Sci. **37**, 693–702 (1980).

[14] K. Olsen, "Orientation measurements of cod in Lofoton obtained from underwater photographs and their relation to target strength," ICES C.M. B:17 (1971).

[15] O. Nakken and K. Olsen, "Target strength measurements of fish," Rapp. P.-v. Reun. Cons. Int. Explor. Mer. **170**, 52–69 (1977).

[16] K. G. Foote, and E. Ona, "Tilt angles of schooling penned saithe," J. Cons. Int. Explor. Mer. **43**, 118–121 (1987).

[17] K. G. Foote, "Averaging of fish target strength functions," J. Acoust. Soc. Am. **67**, 504–515 (1980).

[18] K. G. Foote, "Rather-high-frequency sound scattering by swimbladdered fish," J. Acoust. Soc. Am. **78**, 688–700 (1985).

[19] K. G. Foote and J. J. Traynor, "Comparison of walleye pollock target strength estimates determined from *in situ* measurements and calculations based on swimbladder form," J. Acoust. Soc. Am. **83**, 9–17 (1988).

[20] I. Everson, "Some aspects of small scale distribution of *Euphausia superba*," Polar Biol. **8**, 9–15 (1987).

[21] K. G. Foote, I. Everson, J. L. Watkins, and D. G. Bone, "Target strengths of Antarctic krill (*Euphausia superba*) at 38 kHz and 120 kHz," J. Acoust. Soc. Am. **87**, 16–24 (1990).

[22] D. Chu, T. K. Stanton, and P. H. Wiebe, "Frequency dependence of sound backscattering from live individual zooplankton." ICES J. Mar. Sci. **49**, 97–106 (1992).

[23] C. F. Greenlaw, "Backscattering spectra of preserved zooplankton," J. Acoust. Soc. Am. **62**, 44–52 (1977).

[24] P. H. Wiebe, C. H. Greene, T. K. Stanton, and J. Burczynski, "Sound scattering by live zooplankton and micronekton: Empirical studies with a dual-beam acoustical system," J. Acoust. Soc. Am. **88**, 2346–2360 (1990).

[25] R. E. Pieper, D. V. Holliday, and G. S. Kleppel, "Quantitative zooplankton distributions from multifrequency acoustics," J. Plankton Res. **12**, 433–441 (1990).